Photothermal phenomenon: Extended ideas for thermophysical properties characterization

Cite as: J. Appl. Phys. 131, 065107 (2022); https://doi.org/10.1063/5.0082014 Submitted: 11 December 2021 • Accepted: 23 January 2022 • Published Online: 11 February 2022

🔟 Jing Liu, 🔟 Meng Han, 🔟 Ridong Wang, et al.

COLLECTIONS

Paper published as part of the special topic on Non-Invasive and Non-Destructive Methods and Applications Part I â



This paper was selected as an Editor's Pick







ARTICLES YOU MAY BE INTERESTED IN

Tutorial on broadband transmissive metasurfaces for wavefront and polarization control of terahertz waves

Journal of Applied Physics 131, 061101 (2022); https://doi.org/10.1063/5.0077652

The effect of strain and pressure on the electron-phonon coupling and superconductivity in MgB₂-Benchmark of theoretical methodologies and outlook for nanostructure design

Journal of Applied Physics 131, 063902 (2022); https://doi.org/10.1063/5.0078765

Influence of the absorption layer on the pulsed laser (355 nm) annealing thermal budget during formation of Ni-based ohmic contacts on 4H-SiC substrate

Journal of Applied Physics 131, 065108 (2022); https://doi.org/10.1063/5.0076822





Photothermal phenomenon: Extended ideas for thermophysical properties characterization



Cite as: J. Appl. Phys. 131, 065107 (2022); doi: 10.1063/5.0082014 Submitted: 11 December 2021 · Accepted: 23 January 2022 · Published Online: 11 February 2022















AFFILIATIONS

¹College of New Materials and New Energies, Shenzhen Technology University, Shenzhen, Guangdong 518116, People's Republic of China

²Shenzhen Institute of Advanced Electronic Materials, Shenzhen Institute of Advanced Technology, Chinese Academy of Sciences, Shenzhen, Guangdong 518055, People's Republic of China

³State Key Laboratory of Precision Measuring Technology and Instruments, Tianjin University, Tianjin 300072, People's Republic of China

 4 School of Mechanical and Automotive Engineering, Shanghai University of Engineering Science, Shanghai 201620, People's Republic of China

Department of Mechanical Engineering, Iowa State University, 271 ASC II, 1915 Scholl Road, Ames, Iowa 50011, USA

Note: This paper is part of the Special Topic on Non-Invasive and Non-Destructive Methods and Applications Part I: Festschrift.

a)Authors to whom correspondence should be addressed: shxu]6@sues.edu.cn and xwang3@iastate.edu

ABSTRACT

The photothermal phenomenon involves material photon heating in the form of continuous waves, modulated waves, or pulses. The resulting temperature rise carries very rich information about the material's structures and thermophysical properties. This review is constructed to cover some of the extended ideas of the photothermal phenomenon for measuring a material's thermophysical properties and interface thermal conductance/resistance. For frequency-domain photothermal phenomena, the photoacoustic (PA) and photothermal radiation (PT) techniques provide great ways to measure coatings and suspended samples, which can also be measured using the laser flash and timedomain thermoreflectance (TDTR) techniques. Thermal probing based on electrical thermal sensing is successfully implemented in the transient photo-electro-thermal (TPET) and pulsed laser-assisted thermal relaxation (PLTR) techniques, which significantly extend the capability of laser flash technique to micro/nanoscale 1D structures. The energy transport state-resolved Raman (ET-Raman) is distinct from traditional techniques in its material-specific thermal sensing capability and integral way of ultrafast thermal sensing. Detailed physics discussions are provided for all these techniques, including their advantages and limitations. Still, large development rooms exist for the relatively new techniques, including TPET, PLTR, and ET-Raman. These include measurements under extreme situations, sensitivity improvement, and distinguishing conjugated physical processes.

Published under an exclusive license by AIP Publishing. https://doi.org/10.1063/5.0082014

I. INTRODUCTION

The photothermal phenomenon involves the general idea that a material will experience a temperature rise upon photon heating. The photon absorption mostly occurs in a very small region beneath the material surface, so in many situations, it is treated as surface heating. Such treatment could significantly simplify the physical analysis while not sacrificing much accuracy. When the material has a quite long optical absorption depth, the photon

penetration depth becomes large. Still, the relative importance of volumetric absorption depends on the physical process under consideration, e.g., material size, time scale, and the location where the temperature rise is sensed. For the involved photon, it could be normal light of a wide spectrum, or laser light of a very narrow spectral linewidth (e.g., those used in Raman spectroscopy for concurrent heating). Also, the light can be a continuous wave (CW), amplitude modulated at well-designed frequencies (f), or pulses. The temperature rise occurring in the photothermal process can be

probed by sensing various physical phenomena it causes, like the acoustic signal in photoacoustic techniques, ¹⁻⁶ surface thermal emission, ⁷⁻¹⁰ electrical resistance change, ^{11,12} spectroscopy wavenumber shift, ¹³⁻¹⁵ and surface optical properties change. ^{16,17} The temperature rise during the photothermal process in fact is determined by various properties, including the light intensity, time of heating, and thermophysical properties of the sample. It has prompted a large number of great applications, including bioimaging, ¹⁸ non-destructive evaluation of material defects, ¹⁹⁻²³ photothermal spectroscopy for gas sensing, ^{24,25} and thermophysical properties measurement. ^{12,26,27}

All the aforementioned applications deeply involve the heat transfer process in the sample under photon heating. Such a process is tightly related to the photon heating patterns in spatial and temporal domains, thermophysical properties of the material, its defects, and the ambient conditions. This paper is not intended to provide a comprehensive review of the photothermal phenomenon and its applications. Rather it focuses on thermophysical properties measurement using the general and extended ideas of the photothermal phenomenon. This phenomenon causes other physical phenomena which are quite sensible and feature unique advantages. These extended photothermal ideas make it possible to measure thermophysical properties, like thermal conductivity (κ) , specific heat (ϵ_p) , thermal diffusivity (α) , and structure domain sizes down to the atomic level.

In this paper, we provide an in-depth review of the photoacoustic and photothermal techniques (Fig. 1) in Sec. II, transient photo-electro-thermal techniques in Sec. III including the transient photo-electro-thermal technique (Fig. 2) and pulsed laser-assisted thermal relaxation techniques (Figs. 3 and 4), time-domain thermoreflectance technique (Fig. 5) in Sec. IV, and micro/nanoscale thermal characterization using Raman spectroscopy by controlling the energy transport states (Sec. V). This section covers the time-domain differential Raman (Fig. 7), frequency-resolved Raman (Fig. 8), and energy transport state-resolved Raman (Fig. 9). The review consists of a fundamental physics introduction, discussions on thermal characterization capabilities and limitations, and an outlook for future research directions.

II. PHOTOACOUSTIC AND PHOTOTHERMAL RADIATION TECHNIQUES FOR THERMAL CHARACTERIZATION OF COATINGS: DOWN TO SUB- μ M SCALE

A. Physical model development

The photoacoustic (PA) and photothermal radiation (PT) techniques discussed here belong to a large branch of laser-assisted noncontact thermal measurement technologies. They all involve surface laser heating and use surface temperature information to extract thermophysical properties of the material under study. They are mostly utilized for the thermal probing of the multilayered structure beneath the surface. The PA and PT techniques share the same rationale for thermal measurement as shown in Fig. 1(a). An amplitude-modulated laser (duty of 50%) is employed as a heating source to heat the tested sample from its surface. During each heating period, the surface of the sample absorbs the incident photon energy and generates heat. Assuming that the sample has a much larger thermal conductivity than its ambient gas which is true under most scenarios, heat will be dominantly conducted

along the thickness direction to the bottom. The surface thermal response to the heating condition, including time delay and amplitude, is ascribed to the thermophysical properties and interfacial thermal conductance in the heating depth of the sample. By varying the modulation frequency, one could control the heating depth to evaluate the thermophysical properties of the layer of interest beneath the surface. To detect this thermal response, the PA technique is based on the work done by the heated surface. The periodical thermal expansion of the heated surface does work on the adjacent gas²⁸ and raises a sound wave/pressure variation that could be detected in the form of an acoustic signal. ^{2,29–31} The PT technique advances the measurement by directly measuring the thermal radiation from the heated surface. ^{9,10,32}

The typical experimental setups for PA and PT techniques are shown in Figs. 1(b) and 1(c). Generally, there is a modulated laser slightly focusing on a large spot on the sample surface to guarantee that the thermal diffusion length in both gas and the sample is much shorter than the diameter of the laser spot and the in-plane heat conduction in all layers could be safely neglected. The PA technique employs a microphone to detect sound waves [Fig. 1(b)], while the PT technique uses an infrared detector [Fig. 1(c)] to detect the temperature variation on the surface by measuring the thermal radiation. The acoustic/thermal radiation signal is finally gathered by a lock-in amplifier, and only the frequency-locked one is recorded for further thermal analysis.

The physical model (RG model) to describe the heat transfer in the PA technique was first developed by Rosencwaig and Gersho¹ to depict the temperature variation, in which only the thermophysical properties of each layer were considered. Wang et al. improved the model to additionally evaluate the effect of interface thermal conduction on surface temperature response. As shown in Fig. 1(a), the layers numbered from 1 to N are sample layers between the substrate (layer 0) and the gas layer (layer N+1). Each layer (for example, layer i) has a thickness of $L_i = l_i - l_{i-1}$. Other thermophysical properties of layer i are denoted as: thermal conductivity κ_i , specific heat $c_{p,i}$, thermal diffusivity α_i , and optical absorption coefficient β_i . The thermal contact resistance between layer i and (i+1) is $R_{i,i+1}$. Other parameters needed in the physical model are the thermal diffusion length $\mu_i = \sqrt{\alpha_i/\pi f}$ and thermal diffusion coefficient $a_i = 1/\mu_i$, when f denotes the modulation frequency of the incident laser. The governing equation for 1D thermal diffusion in layer i can be expressed as

$$\frac{\partial^{2} \theta_{i}}{\partial x^{2}} = \frac{1}{\alpha_{i}} \frac{\partial \theta_{i}}{\partial t} - \frac{\beta_{i} I_{0}}{2\kappa_{i}} \exp\left(\sum_{m=i+1}^{N} -\beta_{m} L_{m}\right) \times e^{\beta_{i}(x-l_{i})} (1 + e^{j\omega t}), \quad (1)$$

where $\theta_i = T_i - T_{amb}$ is the temperature rise of layer i and T_{amb} is the ambient temperature. ω is the angular frequency $(2\pi f)$ corresponding to the modulation frequency f. The detailed derivation for solving Eq. (1) has been reported in Ref. 28. The resulting temperature rise θ_i has three components: the transient component $\theta_{i,t}$ that will go to zero after the sample surface reaches the steady state, the steady DC component $\overline{\theta}_{i,s}$, and the steady AC component $\widetilde{\theta}_{i,s}$ which will vary with the modulation frequency. Thus, only $\widetilde{\theta}_{i,s}$ will be collected by the lock-in amplifier. Its

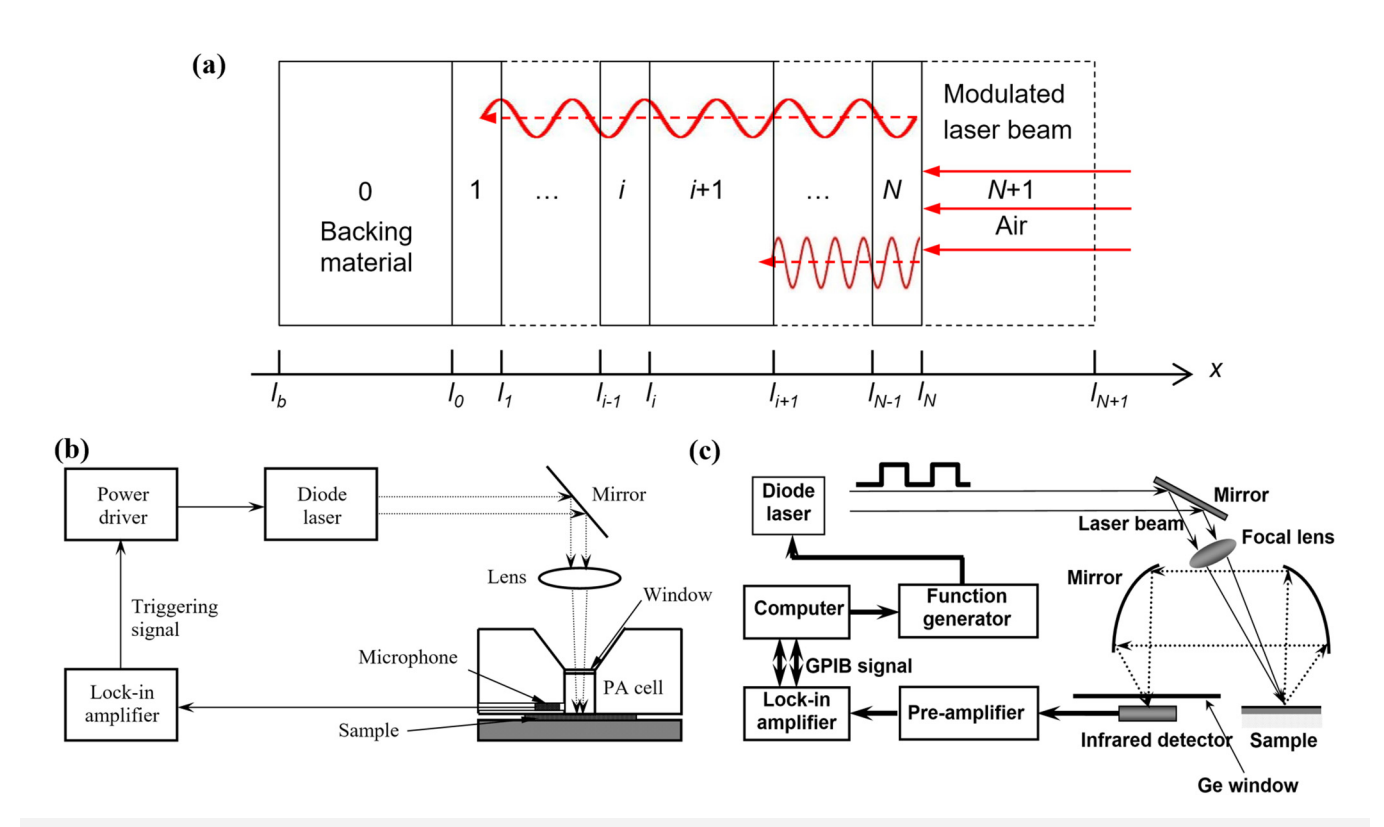


FIG. 1. (a) Physical schematics of the PA/PT techniques. (b) Typical experimental setup for the PA technique. Reproduced with permission from Hu *et al.*, J. Appl. Phys. **86**, 3953 (1999). Copyright 1999 AIP Publishing LLC. (c) Typical experimental setup for the PT technique. Reproduced with permission from Wang *et al.*, J. Appl. Phys. **104**, 013528 (2008). Copyright 2008 AIP Publishing LLC.

general solution has an expression as

$$\widetilde{\theta}_{i,s} = [A_i e^{\sigma_i(x-l_i)} + B_i e^{-\sigma_i(x-l_i)} - E_i e^{\beta_i(x-l_i)}] e^{j\omega t}, \tag{2}$$

where $E_i = G_i/(\beta_i^2 - \sigma_i^2)$ with $G_i = \beta_i I_0/(2k_i) \exp\left(-\sum_{m=i+1}^N \beta_m L_m\right)$, and for i < N, $G_N = \beta_N I_0/2k_N$, and $G_{N+1} = 0$. σ_i is defined as $(1+j) \times a_i$ with $j = \sqrt{-1}$.

 A_i and B_i are two important coefficients carrying information about the thermal and optical properties of the sample. They are derived from the interfacial transmission matrix of heating U and the absorption matrix of light for specific adjoining layers. Under the assumption that both the gas layer and backing material are thermally thick $(A_{N+1} = 0 \text{ and } B_0 = 0)$, A_i and B_i have the relation expressed as below at $x = l_i$.

$$\begin{bmatrix} A_i \\ B_i \end{bmatrix} = U_i \begin{bmatrix} A_{i+1} \\ B_{i+1} \end{bmatrix} + V_i \begin{bmatrix} E_i \\ E_{i+1} \end{bmatrix}, \tag{3}$$

where U_i and V_i from layer i + 1 to i are expressed as

$$U_{i} = \frac{1}{2} \begin{bmatrix} u_{11,i} & u_{12,i} \\ u_{21,i} & u_{22,i} \end{bmatrix}; V_{i} = \frac{1}{2} \begin{bmatrix} v_{11,i} & v_{12,i} \\ v_{21,i} & v_{22,i} \end{bmatrix}, \tag{4}$$

where

$$u_{1n,i} = (1 \pm k_{i+1}\sigma_{i+1}/k_i\sigma_i \mp k_{i+1}\sigma_{i+1}R_{i,i+1}) \times exp[\mp\sigma_{i+1}(l_{i+1} - l_i)], \ n = 1, 2,$$
(4a)

$$u_{2n,i} = (1 \mp k_{i+1}\sigma_{i+1}/k_i\sigma_i \mp k_{i+1}\sigma_{i+1}R_{i,i+1})$$

$$\times exp[\mp \sigma_{i+1}(l_{i+1} - l_i)], n = 1, 2,$$
(4b)

$$v_{n1,i} = 1 \mp \beta_i / \sigma_i$$
, , $n = 1, 2,$ (4c)

and

$$v_{2n,i} = (-1 \mp k_{i+1}\beta_{i+1}/k_i\sigma_i \mp k_{i+1}\beta_{i+1}R_{i,i+1}) \times exp[-\beta_{i+1}(l_{i+1} - l_i)], \ n = 1, 2.$$
 (4d)

Thus, the coefficients A_i and B_i are obtained using

$$B_{N+1} = -\frac{\begin{bmatrix} 0 & 1 \end{bmatrix} \sum_{m=0}^{N} \left(\prod_{i=0}^{m-1} U_i \right) V_m \begin{bmatrix} E_m \\ E_{m+1} \end{bmatrix}}{\begin{bmatrix} 0 & 1 \end{bmatrix} \left(\prod_{i=0}^{m-1} U_i \right) \begin{bmatrix} 0 \\ 1 \end{bmatrix}}, \quad (5a)$$

$$\begin{bmatrix} A_i \\ B_i \end{bmatrix} = \left(\prod_{m=i}^{N} U_m\right) \begin{bmatrix} 0 \\ B_{N+1} \end{bmatrix} + \sum_{m=i}^{N} \left(\prod_{k=i}^{m-1} U_k\right) V_m \begin{bmatrix} E_m \\ E_{m+1} \end{bmatrix}.$$
 (5b)

Since the detected thermal radiation is from the surface gas layer (layer N+1), the detected temperature rise has the final expression as

$$\widetilde{\theta}_{N+1,s} = B_{N+1} e^{-\sigma_{N+1} x} e^{j\omega t}. \tag{6}$$

The time delay (phase shift) between the temperature rise and the incident laser is one critical parameter for thermophysical properties evaluation, which is expressed as $Arg(B_{N+1}) - \pi/4$, and the thermophysical properties are included in B_{N+1} . Thus, in the experiment, before measuring the temperature rise of the sample surface, the system is calibrated in advance to determine the phase shift ϕ_{cal} induced by the optical path and equipment. ϕ_{cal} in fact it is the phase shift of the reflected light from the surface in the calibration experiment. Then the measured phase shift ϕ_{raw} is used to obtain the real phase shift as $\phi_{nor} = \phi_{raw} - \phi_{cal}$. ϕ_{nor} and is further compared with theoretically calculated results using trial values of unknown thermophysical properties. The minimum residual implies the best fitted thermophysical properties. The sensitivity of PA/PT based on phase shift is high, as the measurement uncertainty could be controlled at about 5% at the optimized frequency. For a bulk material with a mirror-like surface, the phase shift will always be −45° for PT signal and −90° for PA signal.

The amplitude is another critical parameter for thermophysical properties evaluation, especially having advantages for bulk material measurement where the phase shift carries no useful information. In the PA method, the thermal-variation raised pressure oscillation is detected in the acoustic waveform and has an explicit expression $A = |(1 - \rho)p_{amb}B_{N+1}/\sqrt{2}T_{amb}L_g a_g|$, where ρ is the surface reflectivity, L_g is the typical dimension of the gas cell, a_g is the thermal diffusion coefficient of the gas, and p_{amb} and T_{amb} are the ambient pressure and temperature, respectively. However, the absolute amplitude will be affected by several systematic factors, such as the laser stability, quality of all the reflecting surfaces, the sensitivity of the detector, modulation frequency, etc. To improve the feasibility of the amplitude method, the PT technique employs a normalized amplitude A_{nor} to exclude all the systematic factors and only depends on the thermophysical properties of the sample, $^{8}A_{nor} = A_{raw} \times \sqrt{f}/A_{cal} \approx \zeta/e_{t}$. ζ is a system-related constant across the modulation frequency range and e is the thermal effusivity of the sample with an expression of $e_t = \sqrt{\kappa \rho c_p}$. It reflects the thermal energy needed for 1 K temperature rise in the characteristic thermal diffusion length per unit area per second. Comparing the amplitude method with the phase shift method, the amplitude method has a lower sensitivity, particularly for measuring thermal contact resistance between layers. On the contrary, this insensitivity enables the amplitude method to evaluate thermal conductivity with sound accuracy without knowing the thermal contact resistance. It might be a distinguishing feature for thermal conductivity measurement in a multilayer structure consisting of complex interfaces.

B. Thermophysical characterizations: Capabilities and limitations

The nature of the PA/PT methods is to control the depth of heat conduction along the thickness direction and determine the total thermal resistance involved in the heat conduction. The thermal resistance of layer i is $R_i = L_i/\kappa_i$. If the experiment has a thermal conductivity measurement uncertainty of $\Delta \kappa$, the uncertainty in the thermal resistance measurement will be $\Delta R = L\Delta\kappa/\kappa^2$. When the thermal contact resistance is lower than this value, it will be hard to detect. On the contrary, the thermal resistance of a layer could be hard to measure when the thermal contact resistance is significantly large and its experimental uncertainty (ΔR) is higher than the thermal resistance of the layer. Thus, the largest detectable thermal conductivity of the layer is $L/\Delta R$.

In PA/PT techniques, periodical laser heating is used. Another natural consideration would be pulsed heating and studying a material's thermal response after the pulse. This is the methodology used in the laser flash method, which is another large branch for noncontact laser-assisted thermal measurement. In the laser flash method, a laser pulse irradiates the sample surface and the temperature evolution is detected at the back of the sample.³³ Compared with the laser flash method for the thermal characterization of single-layer material, the PA/PT method could and is good at measuring the thermal conductivity of a specific layer in a multilayer structure besides bulk materials. Also, the thermal response could be collected from either the front or the back. For the laser flash method, new developments also have been reported for measuring multilayer samples and measuring the front surface thermal response.^{34–36} The main difference is that it tracks the material's thermal response after pulsed heating while the PT and PA techniques probe a material's response under periodical laser heating. The delicate phase shift information under different heating frequencies makes PA and PT techniques have unique capabilities for measuring thermophysical properties of layers of different depths (depth profiling).

In most PA/PT measurements, the modulation frequency and light beam size are controlled so the lateral heat conduction in the sample is negligible compared with that in the thickness direction. This will significantly simplify the physical model development, data reduction, and measurement control and accuracy. However, under special scenarios, if the 3D heat conduction needs to be considered, theoretical development needs to consider the laser distribution in space.^{37,38} For thermophysical properties measurement of a coating, although the PA/PT technique can measure the thickness, thermal conductivity, specific heat (ρc_p) , and interface thermal resistance, in fact for the coating itself, only these two combined parameters are independent: L/κ and $L\rho c_p$, where L is the coating thickness. This usually holds true if the modulation frequency is not very high, and the thermal wave can very well penetrate the coating. Physically this is understandable since L/κ and $L\rho c_p$ represent the thermal resistance and heat capacitance the coating has in heat conduction.^{8,32} In other words, if the film thickness is known, the PA/ PT technique can determine the thermal effusivity $e_t = \sqrt{\kappa \rho c_p}$ precisely without any input of thermal conductivity and specific heat. More in-depth discussions and reviews about the PA technique can be found in the book chapter by Wang et al.³

Nevertheless, the PA and PT techniques have limitations. The first problem is the probing depth. In the PA technique, the temperature variation in the front gas stems from two sources: one is the heated surface adjacent to the gas layer and the other is from the work done to the gas layer from surface thermal expansion. The latter one is usually negligible when the modulation frequency is low. However, as the modulation frequency goes higher than the order of 10 kHz, the piston effect by the surface thermal expansion becomes significant and could not be neglected. This will make the theoretical model for temperature rise in the gas layer very complicated in PA measurement. Thus, the PA method is more suitable for the thermal characterization of micrometer thick films and coatings. Another limitation is that the PA technique mainly works at room temperature (due to the limited operating temperature range of the microphone) while the laser flash method is feasible for a wider temperature range. The PT technique can also be applied to higher temperatures. However, for cryogenic states, both the PT and laser flash techniques become difficult to conduct if thermal radiation is still probed for temperature sensing. This is because the peak thermal radiation wavelength is related to temperature as $\lambda_{\text{max}}T = 2989 \,\mu\text{m}$ K (Wien's displacement law).⁴⁰ At low temperatures say 20 K, λ_{max} becomes very long as 0.145 mm, making the detecting very difficult. An alternative way has to be developed to realize very fast and cryogenic temperature sensing. This will be discussed in Sec. III.

III. TRANSIENT PHOTO-ELECTRO-THERMAL CONCEPTS FOR BROAD THERMAL CHARACTERIZATION

In this section, we discuss the techniques based on the concept of laser heating and electrical signal detecting for measuring the thermal transport properties of micro/nanoscale wires and films. Such methodology is intended to overcome technical difficulties faced in PT and laser flash techniques and also extend the measurement capacity to one-dimensional micro/nanoscale structures.

A. Transient photo-electro-thermal (TPET) technique

The first one is the transient photo-electro-thermal (TPET) technique developed in Wang's lab in 2007. 41 In the TPET technique [Fig. 2(a)], the sample (wire or narrow strip) is suspended over two electrodes, and silver paste or Pt deposition is used to secure the electrical and thermal contact. Then, the sample is uniformly irradiated with a CW laser (step function at the startup). The sample will have a temperature rise and finally reach a steady state. How fast the temperature of the sample reaches the steady state is directly related to its thermal diffusivity. In order to detect the temperature rise, a small DC is fed through the sample, where the small change of the electrical resistance/voltage upon laser heating is monitored. Within a moderate temperature rise, it is reasonable to assume that the resistance change is proportional to the temperature rise. Figure 2(a) shows a schematic set up for the TPET experiment. A Wheatstone bridge circuit is used to suppress the noise and improve the sensitivity, where the sample serves as one arm of the bridge. A DC voltage is supplied to the circuit and the bridge voltage is detected with a digital oscilloscope. To make the experiment more efficient, the laser is modulated into square waves, representing the periodical laser on-and-off processes. When the laser is off, the bridge is in a balance status. After the laser is on, the balance will be broken and the voltage variation will be monitored by an oscilloscope. The recorded voltage variation over time is used to determine the thermal transport properties of the sample.

In the TPET experiment, surface heating by the laser will transfer both along and across the sample. However, due to the very large aspect ratio of the sample, the characteristic thermal diffusion time across the sample is much smaller than that along the sample's axial direction. Therefore, it is reasonable to assume the sample has uniform temperature distribution in the cross direction during thermal diffusion along its axial direction. The one-dimensional heat conduction is expressed as the following equation:

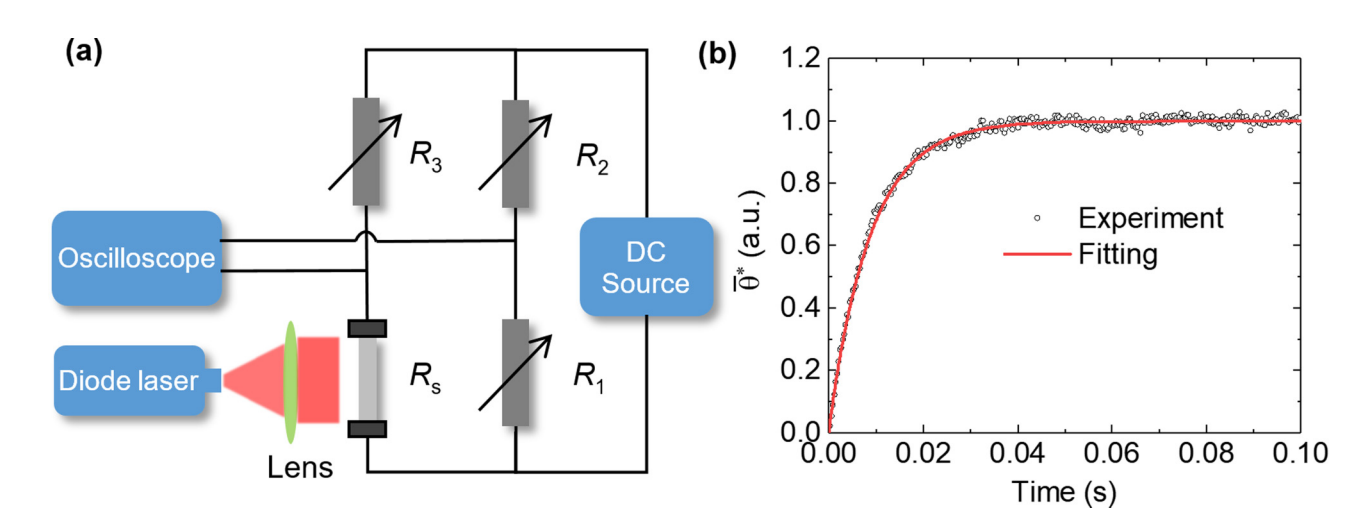


FIG. 2. (a) Schematic setup of the TPET technique. (b) A typical normalized experimental curve and its theoretical fitting for carbon nanotube (CNT) fiber ($80 \,\mu m$ thick and 1.72 mm long) was measured in our lab.

$$\frac{\partial(\rho c_p T)}{\partial t} = \kappa \frac{\partial T^2}{\partial x^2} + \dot{q},\tag{7}$$

where \dot{q} is the equivalent volumetric heat source induced by the laser heating, in the unit of Wm⁻³. The heating effect from DC is constant during the whole measurement and does not affect the transient temperature rising process. ρ , c_p , and κ are the density, specific heat, and thermal conductivity of the sample, respectively. With the help of Green's function, Eq. (7) is solved and the temperature distribution is obtained. The temperature rise is averaged over the suspended sample and then normalized to the steady-state temperature rise. The normalized temperature rise is expressed as the following equation:

$$\bar{\theta}^* = \frac{96}{\pi^4} \sum_{m=1}^{\infty} \frac{1 - \exp[-(2m-1)^2 \pi^2 \alpha_{eff} t/L^2]}{(2m-1)^4},$$
 (8)

where $\bar{\theta}^*$ is the normalized average temperature rise of the suspended sample. α_{eff} is the effective thermal diffusivity of the sample. From Eq. (8), it can be seen that $\bar{\theta}^*$ is only related to the Fourier number $Fo = \alpha_{eff} t/L^2$, which is a dimensionless time containing the combined effects of thermal diffusivity and length for the sample. The effective thermal diffusivity is extracted by fitting the experimental data using this solution. Figure 2(b) shows a normalized temperature rise curve and its analytical fitting for a carbon nanotube (CNT) fiber measured in our lab using the TPET technique. The effective thermal diffusivity is determined as $5.67 \times 10^{-5} \text{ m}^2 \text{ s}^{-1}$. Note this determining effective thermal diffusivity consists of the radiation effect. Rigorous physical models and experimental treatments have been developed to subtract this effect. Such treatments are the same for TPET and transient electrothermal (TET) techniques.

The TPET technique has been successfully applied to measure thermal transport properties of conductive and non-conductive microfibers such as Pt wires, single-wall CNT (SWCNT) bundles, and cloth fibers with a diameter of tens of micrometers. 41 Only for non-conductive samples, a very thin metal coating is needed for electrical signal sensing. Compared with the well-defined TET technique⁴⁵ which uses a DC for sample heating and temperature detecting, the TPET technique provides a more flexible and controllable heating process.⁴¹ Moreover, the much smaller DC in TPET will induce much lower noise, which will also improve the precision of the measurement. Although the TPET technique works well for microfibers, things may be different for nanoscale fibers or films due to their extremely large specific surface area. One concern lies in the effect of radiation heat loss. Reducing the sample length may help to some extent, however, will lead to a much faster temperature rise, especially for samples of high thermal diffusivity. In that case, the time for the sample to reach steady state may be as short as several microseconds, comparable to the rise time of a typically modulated laser. A much faster rise time at a nanosecond scale can be achieved with the help of an electrooptical modulator. Another concern is the contact resistance between sample and electrodes, which may be at the same magnitude as the resistance of the sample itself, especially for a very short sample with a very high thermal conductivity. Such an issue can be addressed by using a much longer sample and well considering the radiation effect. He for the concern of very fast temperature evolution, a pulsed laser can be used and the sample's thermal response is probed by measuring its electrical resistance/voltage change after the pulse heating. Such a concept is similar to the laser flash technique but takes different physics for temperature probing.

B. Pulsed laser-assisted thermal relaxation (PLTR) technique

The PLTR technique is developed in Wang's lab, which is, to some extent, a significant improvement of the TPET technique¹¹ in terms of time response. The experimental setup of the PLTR technique is very similar to that of the TPET technique, including the suspension of the wire or film sample, a small DC, and an oscilloscope for signal measurement [shown in Fig. 3(a)]. The difference is that, instead of the step laser irradiation, a pulsed nanosecond or shorter laser is used for sample heating. During the measurement, the sample will be subject to a sudden temperature increase induced by the pulsed laser, and right after that, the temperature will gradually decrease to the value before the pulse comes in. This thermal relaxation process after the pulsed heating is recorded for thermal diffusivity extraction. Compared with the TPET and TET techniques, the PLTR technique can overcome the rise time limitation of the current source (typically $3 \mu s$) and the modulated laser (typically 10 µs) and can be used to measure samples with short length and high thermal conductivity/diffusivity.

Similar to that in the TPET technique, the thermal transport in the sample can be treated as one-dimensional along the length direction and the governing equation at time t>0 is similar to Eq. (7) except \dot{q} is the volumetric heat source induced by the pulsed laser heating, in the unit of Wm $^{-3}$. Notice that, not like in the TPET technique, where \dot{q} keeps constant when the step laser is on, \dot{q} varies with time and only lasts for a very short time in PLTR. However, the solution to the governing equation is similar. The normalized average temperature evolution is expressed as

$$\bar{\theta}^* = \frac{8}{\pi^2} \sum_{m=1}^{\infty} \frac{\exp[-(2m-1)^2 \pi^2 \alpha_{eff} t/L^2]}{(2m-1)^2}.$$
 (9)

In fact, if both sides of Eq. (7) do first-order derivative to t, it becomes the governing equation for the PLTR technique. Therefore, after first-order derivative to t for Eq. (8), the solution will be the one for PLTR and can be readily proved to be the same as Eq. (9).

Similarly, the normalized average temperature rise is only related to the thermal diffusivity of the sample, which can be extracted by least-square fitting. The PLTR technique has been proved very reliable and precise for determining the thermal diffusivity of Pt wire of $25.4\,\mu\mathrm{m}$ diameter. Further study on CNT bundle and carbon fiber also proved its ability for thermal transport detection with much fast thermal relaxation. Recently, we characterized the thermal transport properties of a stretched polyimide film by employing the PLTR technique. Figure 3(b) shows the normalized experimental data and its fitting curve for measurement along the stretched direction. The thermal diffusivity is determined at $5.32\times10^{-7}\,\mathrm{m}^2\,\mathrm{s}^{-1}$. This proves its excellent ability in testing non-conductive samples.

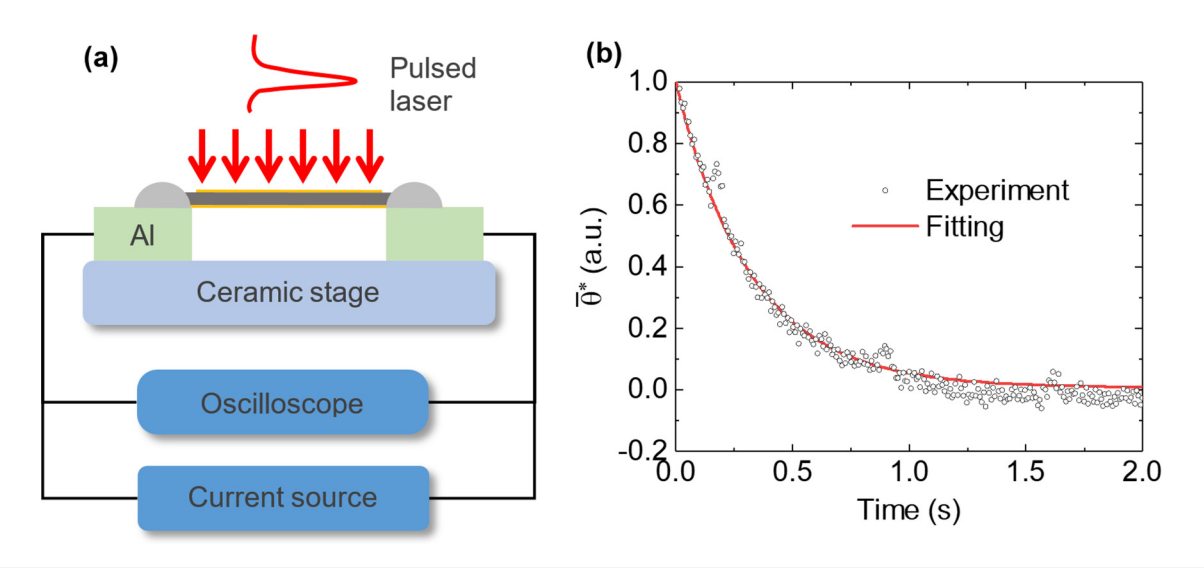


FIG. 3. (a) Schematic setup of the PLTR technique. (b) A typical normalized experimental curve and its theoretical fitting for a polyimide film (20 μm thick and 1.24 mm long).

C. Anisotropic thermal characterization based on PLTR2

The PLTR technique has been further extended to the PLTR2 technique which is able to characterize the thermal transport properties of µm-thick thin films in both the cross-plane and in-plane directions. The experimental setup of the PLTR2 technique is the same as that in the PLTR technique with the pulsed laser heating and the small DC detecting. The difference lies in the sample preparation, which should fulfill the detecting of temperature evolution both in the cross-plane and the in-plane directions. For studying heat transfer in the cross-plane direction, the concept of the laser flash method is introduced, which is heating the film at one surface and detecting the temperature evolution on the other side. To realize this, different strategies are taken for conductive and nonconductive films. For non-conductive films, both surfaces are coated with nanometer thickness Au films, the front surface for laser absorption and the other one for thermal sensing. It is crucial to make sure that only the Au coating at the back surface is connected to the electrical circuit for signal sensing [shown in Fig. 4(a)]. For conductive films, things are a little more complicated. The sensing side of the films should be first coated with a non-conductive film before the Au coating to fulfill the back surface sensing. For heat transfer in the in-plane direction, things are the same as in the aforementioned PLTR technique. Due to the extremely large aspect ratio, it is reasonable to assume that the laser absorbed by the irradiated surface will first transfer to the other side quickly and then dissipate along the in-plane direction [shown in Fig. 4(b)]. This helps determine the thermal transport properties of films in both directions, separately. This technique was first used to study the anisotropic thermal diffusivity of poly(3-hexylthiophene) (P3HT) thin films in 2013. In 2018, Han et al. employed the PLTR2 technique and studied the thermal transport properties of highly conductive graphene papers, partially reduced graphene paper and graphene oxide paper. 48,49 Thanks to the electrical signal detecting strategy, the thermal diffusivity/conductivity in the temperature range from 300 K down to nearly 10 K were measured. This is far beyond the ability of traditional laser flash measurement which uses an infrared detector for signal collection. In these measurements, thermal response as short as a few μ s can be detected with sound accuracy.

IV. TRANSIENT THERMOREFLECTANCE FOR THERMAL CHARACTERIZATION: DOWN TO NM-SCALE

A. Physics of time-domain thermoreflectance (TDTR) technique

In the PT technique discussed in Sec. II, the thermal radiation of the surface is measured for thermal sensing. The surface temperature rise also can affect other optical properties, like surface reflectance. This physical property can be measured by irradiating the surface with a separate laser beam and measuring the change in its reflection. Such a strategy has been used in the time-domain thermoreflectance (TDTR) technique.

TDTR is an optical technique for characterizing the thermal transport of materials. ^{50–53} It is a variation of the optical pump-probe technique, which uses a pump pulse to heat the sample and a probe pulse to detect the optical properties variation due to temperature change. Figure 5(a) shows the schematic of a two-color TDTR system. In the experiment, a Ti-sapphire laser with a high repetition rate (tens of MHz) is used as a heating source. The emitted laser is split into a pump beam for heating and a probe beam for sensing. Before focusing on the sample surface, the pump beam is first modulated by an electro-optic modulator (EOM) with frequencies from a few kHz to a few MHz. An optical time-delay system is used to delay the probe beam, so the probe beam arrives at the sample surface picoseconds to a few nanoseconds later than the pump

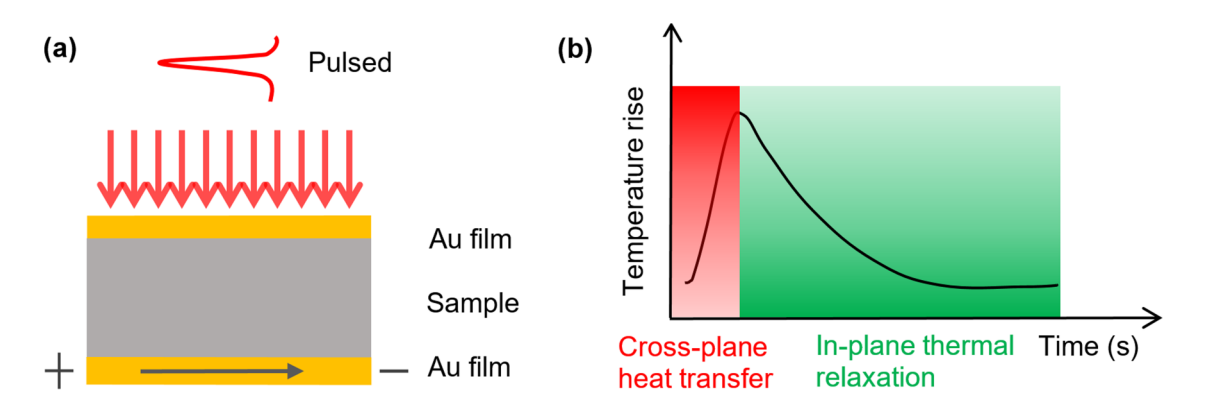


FIG. 4. (a) Schematic of the pulsed laser heating on the Au coated sample. (b) Schematic of the temperature evolution of the back surface Au coating.

beam. The thermoreflectance (*Z*) whose intensity change is proportional to the surface temperature rise is then detected by a photodetector. Typically, the wavelength of the pump beam is chosen to be 800 nm for higher thermoreflectance. In some TDTR setups, the wavelength of the pump beam is frequency-doubled to 400 nm, ⁵⁴ which is aimed to avoid the reflected pump beam entering the detector. Since the TDTR method utilizes the optical reflectivity change rate due to temperature change to detect the

Sample

Half mirror

Objective

Compress

Expand

Beam splitter

Ti: Sapphire

Probe beam

FIG. 5. (a) Schematic diagram of a two-color TDTR system. Only key components are shown in the diagram. (b) Configuration of the sample (not to scale). The gray, orange, and blue layers are transducer (Al or Au), thin-film, and substrate, respectively.

thermal response of materials, a metal film as a transducer is coated on the sample surface. Al and Au's films are the two most commonly-used transducers.⁵⁵ Figure 5(b) shows a typical configuration of the sample.

For a sample under heating in TDTR measurement, the governing equation of the 3D heat conduction model in cylindrical coordinate can be expressed as

$$\frac{\kappa_r}{r} \frac{\partial}{\partial r} \left(r \frac{\partial T}{\partial r} \right) + \kappa_z \frac{\partial^2 T}{\partial z^2} = \rho c_p \frac{\partial T}{\partial t},\tag{10}$$

where κ_r and κ_z are the in-plane and cross-plane thermal conductivity. T is the temperature. ρ and c_p are the density and specific heat capacity of the sample. Since the penetration depth of the thermal wave is far less than the substrate thickness, the substrate can be considered semi-infinite. Thus, the boundary condition is that the bottom surface of the substrate is adiabatic. After solving the above equation, considering the Gaussian distribution of the pump beam and probe beam, the thermoreflectance frequency response to a single pulse in Hankel transform $[H(\omega)]$ can be expressed as 54

$$H(\omega) = \frac{Q}{2\pi} \int_{0}^{\infty} k\left(\frac{-D}{C}\right) \exp\left[\frac{-k^2(w_0^2 + w_1^2)}{8}\right] dk, \tag{11}$$

where Q is the power of the pump beam. k and ω are Hankel transform variables and frequency. w_0 and w_1 are the $1/e^2$ radii of the pump and probe beam. C and D are the components of the transfer matrix which is determined for a specific structure. ⁵⁶ Since the decay time of the measured signal and the interval time (t_p) between pump pulses are comparable, the thermoreflectance response (Z) is the accumulation of single pulse response $H(\omega)$ and can be expressed as ⁵⁶

$$Z(\omega_0) = V_{in} + iV_{out} = \frac{\beta QQ_{probe}}{T^2} \sum_{k=-\infty}^{k=\infty} H(\omega_0 + k\omega_s) e^{ik\omega_s \tau}, \quad (12)$$

where V_{in} and V_{out} are the real and imaginary parts of the response. They are extracted by a lock-in amplifier. β is a constant which

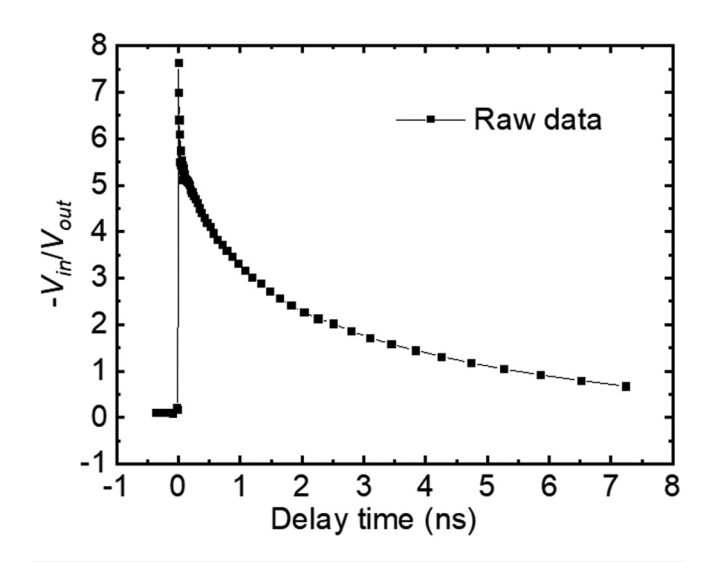


FIG. 6. Typical raw data for Al-coated c-Si₃N₄ crystal as the sample in TDTR experiment, $-V_{in}/V_{out}$ was set as the fitting parameter.

includes the gain of the photodetector, thermoreflectance coefficient of the transducer, and reflectivity of the pump beam and probe beam. Q_{probe} is the power per pulse of the probe beam. ω_s is the laser repetition frequency. t_p is the interval time between the pump pulse and is equal to $2\pi/\omega_s$. Figure 6 shows our raw data of an Al-coated c-Si₃N₄ crystal measured using TDTR. Usually, $-V_{in}/V_{out}$ is set as the fitting parameter as it is a more robust parameter than V_{in} .⁵⁷

B. Advantages and disadvantages of TDTR

In TDTR, the delay time is in a range of a few picoseconds to a few nanoseconds by varying the optical path lengths of the probe beam. As a result, an extremely high time resolution can be achieved. The spatial resolution of TDTR can be as small as a few microns. The advantages of TDTR include simple sample preparation and the versatile capability of determining multiple thermophysical properties. With all the advantages, TDTR has been widely employed in characterizing the thermal conductivity of samples from the nanoscale to the macroscale.⁵⁸⁻⁶³ The thermal penetration depth in TDTR in fact is determined by the pulse interval (t_p) . For a 50 MHz repetition rate, we have $t_p = 20 \text{ ns}$, which represents the very typical optical delay upper limit in TDTR. Immediately after one pulse, although the detected temperature decay also has effects from previous pulses, such effects are quite weak. Therefore, the thermal penetration depth (d_z) in the z-direction is defined as $d_z = \sqrt{t_p \kappa_z/(\rho c_p)}$. For a thermal diffusivity range of 10^{-7} – 10^{-4} m² s⁻¹, d_z is in the range of 3×10^{-8} to 10^{-6} m. This means for a coating thicker than $1 \mu m$, its interface thermal resistance becomes difficult to measure. Compared with the PT technique mentioned above, TDTR has a higher sensitivity for measuring very thin coatings (~nm thick), while the PT can vary the modulation frequency from a few Hz to sub-MHz and is capable of measuring sub-micrometer or thicker coatings and interface thermal resistances. As the laser spot size is larger, the thermal measurement is more sensitive to cross-plane thermal conductivity, while when the spot size is smaller, the thermal measurement is sensitive to both cross-plane and in-plane thermal conductivities. By employing a variable laser spot size approach, the TDTR can characterize the thermal conductivity of materials with strong anisotropy. ^{58,64} To obtain reasonable thermal conductivity of 2D materials, the thickness of 2D materials should be larger than 100 nm. ⁶⁵ As a result, TDTR is not very physically suitable for measuring the thermal conductivity of few-layered 2D materials.

The feasibility of TDTR for thermal measurement depends on the temperature-related surface reflectance. If a surface material is optically opaque, this measurement has no problem in terms of measurement and physical model development since the signal is very well defined. However, for optically transparent material on a substrate, the situation becomes very challenging. For instance, if a 2D material (usually <nm to a few nm thick) is placed on a substrate, then the surface reflectance will be affected by temperatures of both the 2D material and substrate, but the signal cannot differentiate this effect. Normal treatment by depositing a metallic film on the 2D material (making a sandwich structure) will significantly change the morphology of the 2D material, its interface structure, and the local thermal transport properties. To overcome this challenge, Raman spectroscopy has become a widely adopted alternative to realize material-specific thermal sensing. That is, the temperature sensed by Raman spectroscopy can be precisely referred to as a specific sample since different materials have different Raman spectra, which could be termed as their "fingerprint."

V. ENERGY TRANSPORT STATE-RESOLVED RAMAN MEASUREMENT: DOWN TO ATOMIC LEVEL

Raman spectroscopy, which carries signature thermal information about materials, is widely used in thermophysical characterization. Currently, many different Raman-based methods have been proposed for constructing different energy transport states in spatial and time domains. Among these methods, the steady-state Raman technique is the most widely used one. For this technique, a continuous-wave laser is used for both heating and Raman probing. And, the interface thermal resistance (R) between the sample and the substrate or thermal conductivity (κ) is measured by collecting the Raman signals under different laser powers and temperatures. ^{66–69} In the measurement, both temperature calibration and laser absorption evaluation, which are time-consuming and have a high uncertainty, are conducted to realize a relatively low-accuracy determination of R or κ .

A. Raman-based thermal probing in time and frequency domains

The time-domain differential Raman (TD-Raman) technique, 70,71 which is inspired by the TET technique, is proposed to realize effective thermal characterization of one-dimensional (1D) or 2D materials by using a square-wave modulated laser of varying duty cycles for both sample heating and thermal probing. Both steady-state and transient heating states are constructed for this technique. The transient heating includes a laser excitation time (t_c) and a thermal relaxation time (t_r) , in which a long enough

period of t_r is needed for the complete cooling down of the sample before the next cycle. Taking a silicon cantilever as an example, one end is connected to the base and the other end is heated by a modulated laser. Raman signal variations, which are linearly related to the temperature rise of the sample, are utilized to characterize the average temperature rise of the sample under laser heating. Then, the normalized accumulative Raman emission within one cycle is determined based on the below equation:

$$E_{\omega}^{*}(\omega, F_{o,e}) = \frac{I_{0}}{F_{o,e}} \int_{0}^{F_{o,e}} (1 - A\Delta \overline{T}^{*})$$

$$\times \exp \left[-\frac{4 \ln 2 \times (\omega - \omega_{0} + B\Delta \overline{T}^{*})}{(\Gamma_{0} + C\Delta \overline{T}^{*})2} \right] dFo, \quad (13)$$

where I_0 , ω_0 , and Γ_0 are the corresponding Raman intensity, Raman shift, and linewidth at the beginning of laser heating, A, B, C are the changing rates of these three parameters, and $Fo = \alpha t/L^2$ is the Fourier number.

As shown in Figs. 7(a) and 7(b), the normalized Raman intensity and Raman wavenumber decrease quickly with the rapid temperature rise at the beginning of laser heating. Under constant laser heating, these two parameters reach constant values when a steady state is reached. Based on Eq. (13), the thermal diffusivity (α) of the silicon cantilever is determined by trying different values of α to obtain the best theoretical curve fitting of the experimental results. Although both temperature rise and laser absorption coefficient are not required for this technique, a distinct problem is that it needs enough time to collect the Raman signal which makes it very difficult to be used for very fast thermal transport characterization.

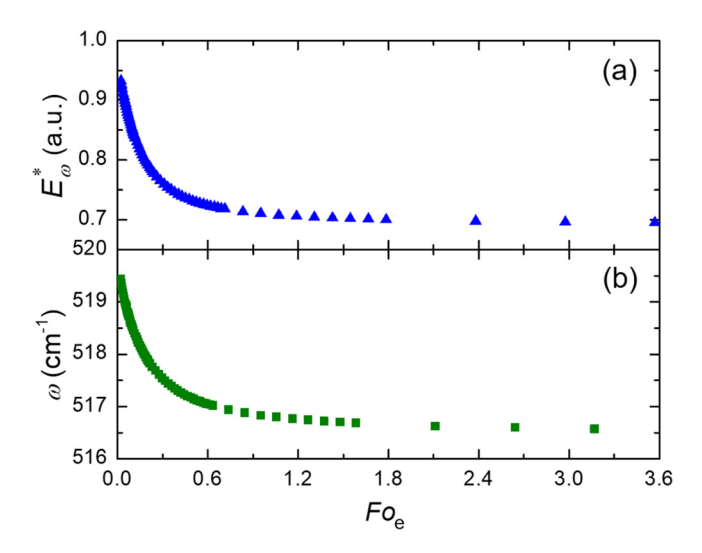


FIG. 7. (a) The decreasing trend of the normalized Raman intensity against the Fourier number. (b) The decreasing trend of the Raman wavenumber against the Fourier number. Reproduced with permission from Xu *et al.*, Opt. Express **23**, 10040 (2015). Copyright 2016 The Optical Society.

B. Raman probing with designed energy transport states

The frequency-resolved Raman (FR-Raman) technique, 72 which uses an amplitude-modulated square-wave laser with different modulation frequencies, can solve the problem in TD-Raman while maintaining the same-level measurement accuracy. As shown in Fig. 8(a), the laser excitation time and the thermal relaxation time are equal. For this technique, two extreme situations, which are very high frequencies and very low frequencies, are shown in Figs. 8(b) and 8(c), are considered for physics explanation. It is found that the temperature rise values at these two states (ΔT_{as} and ΔT_s) are related as $\Delta T_{qs} = \Delta T_s/2$, which indicates that the temperature rise values increase with the decrease of frequency. The variation of corresponding Raman signals against modulation frequency is used to determine the sample's α . In addition, the FR-Raman technique is a good candidate for measuring the thermal conductivities of materials with in-plane anisotropy, such as black phosphorus, 73 etc. However, as the data fitting of this method uses Raman signals against the modulation frequency, it means the experiments should be conducted under many different frequencies. This makes the technique quite laborious.

The frequency-domain energy transport state-resolved Raman (FET-Raman) technique, ¹⁵ in which a fixed frequency is used, is proposed to address the above challenge. For this technique, both steady-state and transient state heating are constructed. By using different laser powers (P), two Raman shift coefficients (RSC), $\psi_{\rm CW} = \partial \omega / \partial P = \beta \times (\partial \omega / \partial T) \times f_1(\kappa)$ and $\psi_{\rm FR} = \partial \omega / \partial P = \beta \times (\partial \omega / \partial T) \times f_2(\kappa)$ and $\psi_{\rm FR} = \partial \omega / \partial P = \beta \times (\partial \omega / \partial T) \times f_2(\kappa)$ are obtained under two heating states. Due to the different thermal diffusion lengths in the two states, a dimensionless normalized RSC $\Theta = \psi_{\rm FR}/\psi_{\rm CW} = f_3(\kappa, \rho c_p)$, which can eliminate the effect of laser absorption coefficient (β) and Raman shift temperature coefficient ($\partial \omega / \partial T$), is obtained to determine the in-plane thermal conductivity (κ) of 2D materials. This technique can also be used to characterize the anisotropic thermal conductivity of carbon fibers in combination with the TET technique.

It can be seen all the aforementioned three techniques (TD-Raman, FR-Raman, and FET-Raman) construct the heating states in time domains. Similarly, the heating states can also be varied in spatial domains. Yuan et al. 75 developed an energy transport state-resolved Raman (ET-Raman) technique by constructing five states in both time and spatial domains to measure κ , R, and hot carrier diffusion coefficient (D) of MoS₂ nanofilms on c-Si. The physical principle of this technique is shown in Fig. 9. Under laser irradiation, hot carriers are generated and diffuse in space before they recombine with holes. Then, the energy from hot carriers is transported by phonons through heat conduction, which is κ -dependent. In addition, the energy is also transported from MoS₂ to c-Si, which is determined by interface thermal resistance R. Similarly, three dimensionless normalized RSCs, which are functions of R, D, and κ , are obtained to realize the simultaneous determination of these three properties. In the five-state ET-Raman technique, a picosecond laser is used to realize the transient heating, which is good for supported samples but will cause strong heat accumulation in suspended samples because of the very short pulse interval. A nanosecond laser can be used instead to realize the thermophysical characterization of suspended samples. Zobeiri et al.⁷⁶

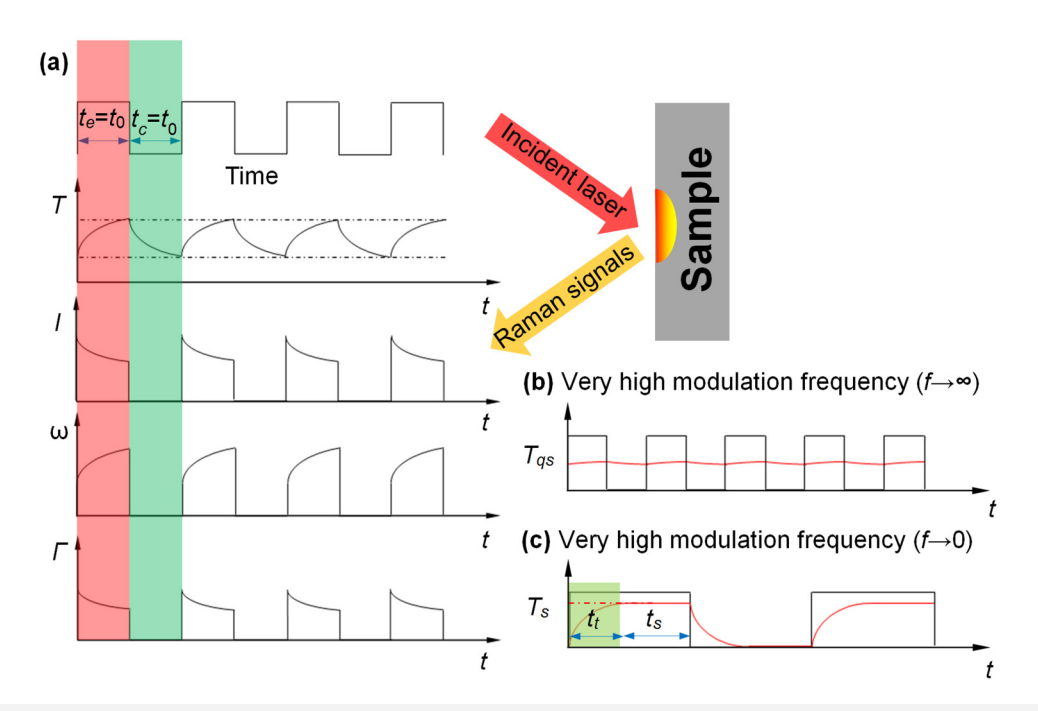


FIG. 8. (a) Mechanism of the FR-Raman technique. (b) Temperature variation at a very high modulation frequency. (c) Temperature variation at a very low modulation frequency. Reproduced with permission from Wang et al., Opt. Lett. 41, 80 (2016). Copyright 2016 The Optical Society.

proposed a three-state nanosecond ET-Raman technique to measure κ and D of suspended WS₂ nanofilms. For this technique, one steady heating state and two transient heating states with different local heating sizes are constructed.

C. Energy carrier-wide thermal nonequilibrium

All the above techniques are based on the Raman spectrum of samples, which indicates that it is of great importance to study the complicated physical processes happening inside these Raman-based techniques. In short, the process is the energy transfer among photons, electrons, and phonons, as shown in Fig. 10(a). The phonons consist of three optical branches and three acoustic branches, which are longitudinal optical (LO), transverse optical (TO), flexural optical (ZO), longitudinal acoustic (LA), transverse acoustic (TA), and flexural acoustic (ZA) branches. Under laser excitation, the temperatures of all these branches are different. ZA phonons are the main heat carriers for heat conduction, while Raman signals are related to the three optical phonons (OP) branches. However, the temperature differences among these phonon branches are ignored in all the previous Raman-based techniques, which could lead to a significant underestimation of thermal properties.

As shown in Fig. 10(a), OPs transfer the majority of the energy to acoustic phonons (APs) through phonon coupling. Figure 10(b) shows that the temperature difference between OP and AP (ΔT_{OA}) decreases to zero faster than the temperature rise of AP (ΔT_{AP}), which means that phonon coupling between OP and

AP is negligible under a very large laser spot. Figure 10(c) shows the temperature rise of OP (ΔT_m), which is expressed as ΔT_m $= \Delta T_{OA} + \Delta T_{AP} \propto A r_0^{-2} + f(\kappa) \times r_0^{-n} \ (n < 2) \text{is determined based}$ on the Raman signals under different local heating sizes. Based on this mechanism, for the first time, Wang et al. 14 developed a sixstate nanosecond ET-Raman to explore the temperature nonequilibrium among these phonon branches experimentally. In this technique, three steady heating states and three transient heating states are constructed by varying the local laser spot size using three objective lenses under continuous-wave laser and nanosecond laser. The phonon coupling factors and the intrinsic κ of MoS₂ and MoSe₂ nanofilms are determined. Afterward, Zobeiri et al. also proposed a novel Raman optothermal technique coupled with a transfer matrix method to characterize the temperature nonequilibrium between OPs and APs. And, R between a nm-thick MoS₂ and substrate is determined by taking this nonequilibrium effect into consideration for the first time. The work by Zobeiri et al.⁷⁸ on graphene paper involved direct measurement of the thermal conductivity using the TET technique and used it to directly calculate the AP temperature rise within the laser heating area. The deviation between this AP temperature rise and the simultaneous Raman-probed temperature rise (OP temperature rise) represents the thermal nonequilibrium between OPs and APs.

For the energy transfer process in 2D materials, attention should also be paid to monolayer transition-metal dichalcogenides (TMDs) with a direct bandgap. In this case, part of the laser-excited electrons recombines with holes radiatively, which is neglected in reported Raman-based techniques resulting in larger

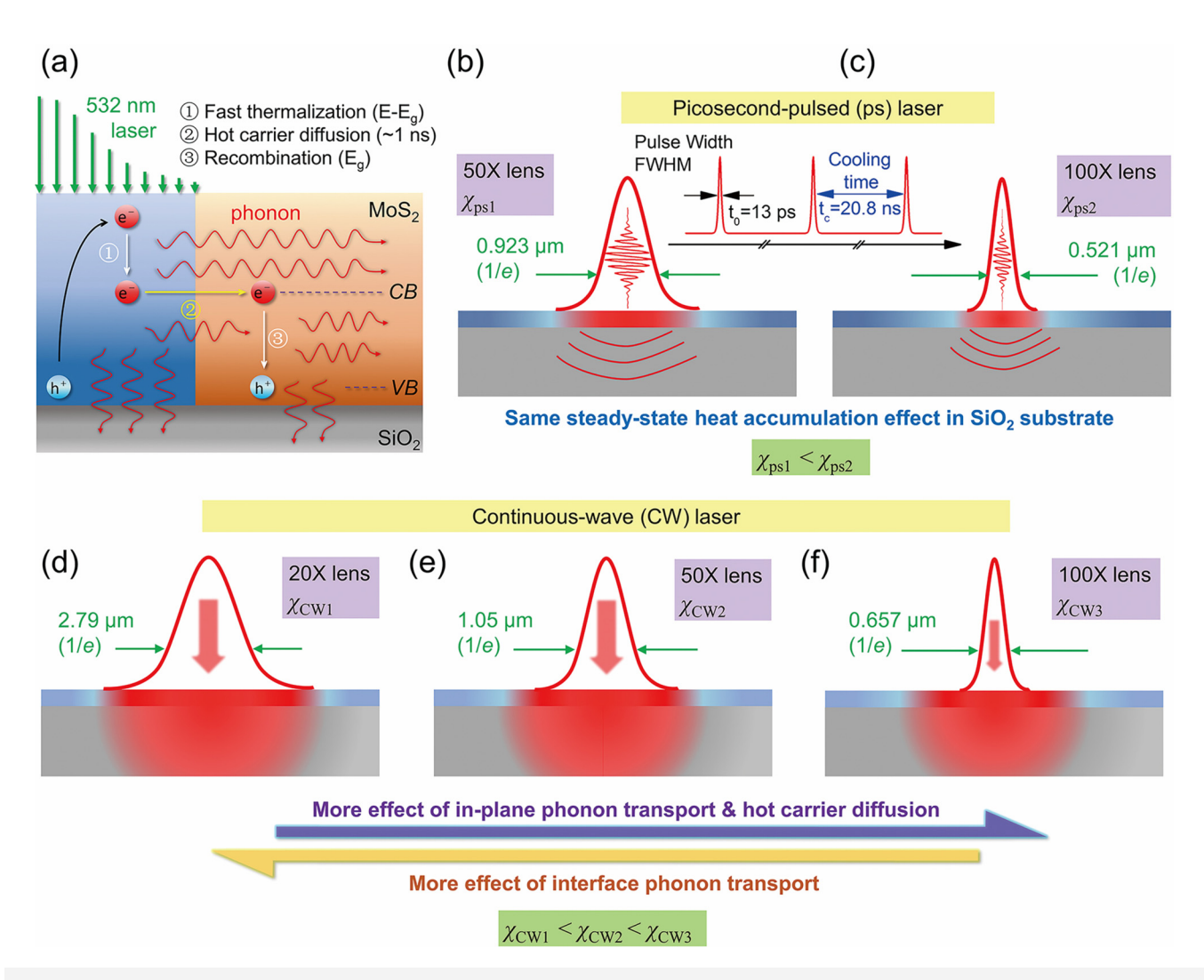


FIG. 9. The mechanism of the five-state energy transport state-resolved Raman (ET-Raman) technique. (a) Physical processes happening in MoS_2 upon laser irradiating. (b) and (c) Two transient states in picosecond laser heating under 50^{\times} and 100^{\times} objective lenses. (d)–(f) Three steady states under CW laser heating with 20^{\times} , 50^{\times} , and 100^{\times} objective lenses. Reproduced with permission from Yuan *et al.*, Phys. Chem. Chem. Phys. **20**, 25752 (2018). Copyright 2018 PCCP Owner Societies.

R. Hunter $et~al.^{79}$ developed a three-state ET-Raman technique to determine R and radiative recombination efficiency (η) of supported monolayer WSe₂ on a fused silica substrate, which is the first known work to take η into consideration on thermal transport characterization of monolayer TMDs. In this technique, one steady heating and two transient heating states are constructed by using a CW laser, a nanosecond laser, and a picosecond laser, respectively. In which, R is determined by using CW laser and nanosecond laser, while η is obtained by using CW laser and picosecond laser. For a more critical and comprehensive review of Raman-based techniques for thermophysical characterization, readers are encouraged to study the recent review by Xu et~al.

In summary, Raman-based techniques show excellent suitability in characterizing thermophysical properties by modulating the

laser in time and spatial domains. 13-15,70-77,79-84 In summary, Raman-based techniques show excellent suitability in characterizing thermophysical properties by modulating the laser in time and spatial domains. In the spatial domain, not only the spot size of the laser can be changed but the shape of the spot size can also be varied, which may be a good methodology to measure materials of in-plane anisotropic thermal conductivities. In addition to the modulation in time and spatial domains, the excitation wavelength of the laser can also be modulated. On one hand, photoluminescence from the sample, the substrate, or the background, can produce noise in order or even greater than the Raman signal. Proper modulation of an excitation wavelength can reduce the detector noise associated with photoluminescence to obtain superior results. On the other hand, the modulation of excitation

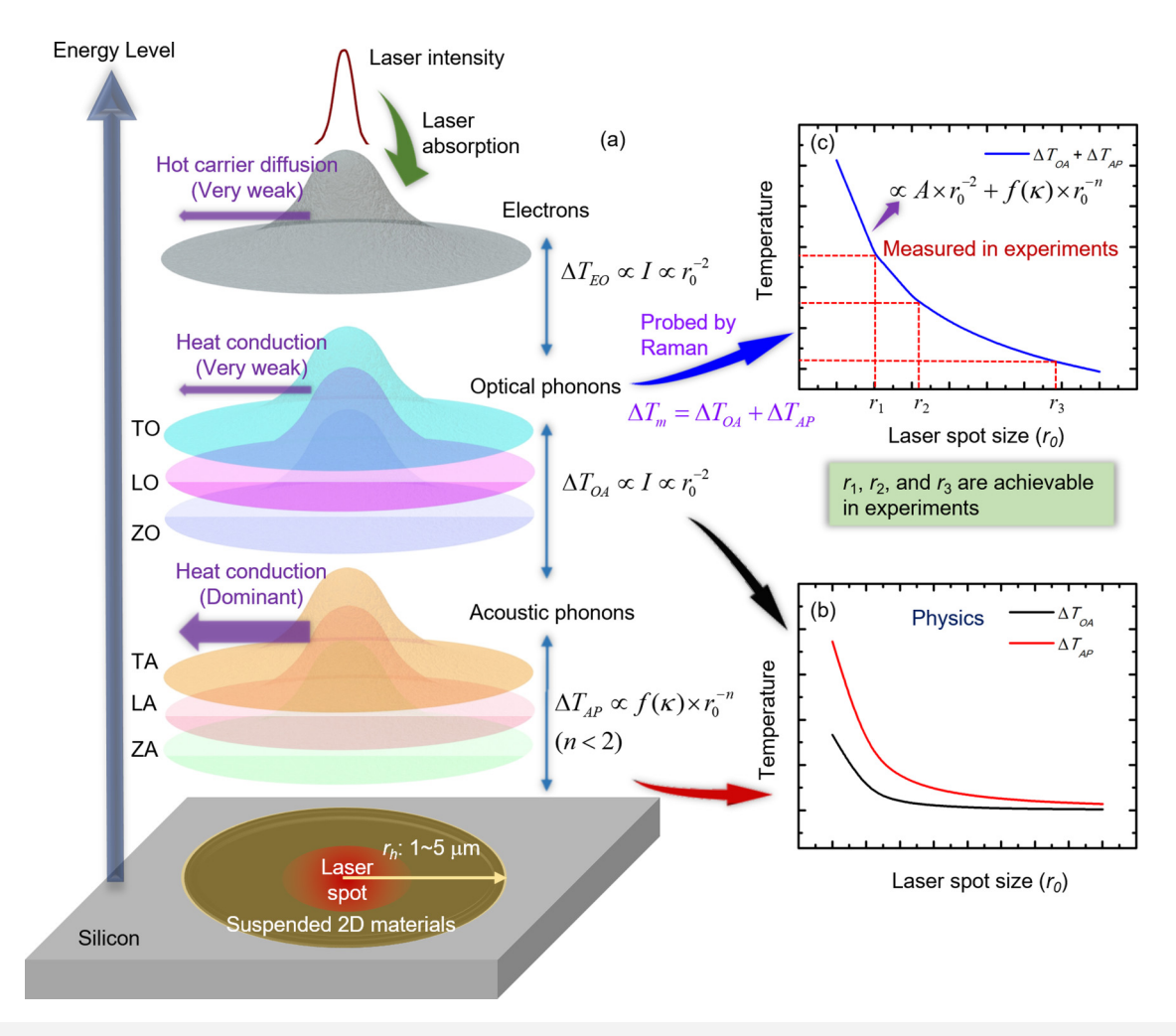


FIG. 10. (a) The cascading energy transfer process among different energy carriers in 2D materials under laser irradiation. (b) The temperature difference between optical phonons and acoustic phonons against laser spot size. (c) The determination of thermal conductivity and energy coupling coefficient between optical phonons and acoustic phonons. Reproduced with permission from Wang *et al.*, Adv. Sci. **7**, 2000097 (2020). Copyright 2020 John Wiley and Sons.

wavelength can realize resonance with an electronic transition of the sample, named resonance Raman spectroscopy, which can provide significantly enhanced signals over normal Raman scattering from the same sample.⁸⁵

VI. DISCUSSIONS AND OUTLOOKS

A. Photothermal energy conversion efficiency

The photothermal phenomenon involves photon energy conversion to heat and temperature rise, which will induce various physical properties to change. Such change is measured for structure and properties characterization. Therefore, the photon-to-heat energy conversion efficiency is an important parameter in the entire process regardless of the absolute temperature rise need in measurement. For many applications, like the ET-Raman technique, such conversion efficiency cannot be controlled since the

material under study needs to be directly irradiated with the laser beam for heating and Raman signal excitation. However, for the PA/PT, TPET, PLTR, PLTR2, and TDTR techniques, the energy conversion efficiency can be significantly improved by coating the sample surface with a layer of very high optical absorption, like amorphous carbon. However, surface properties response to temperature should be kept in mind since a high response is always preferred for temperature sensing. This includes the electrical resistivity temperature coefficient for TPET, PLTR, and PLTR2 techniques. Another example is the surface reflectance consideration for the TDTR technique, which should be as high as possible.

The photon-to-heat energy conversion efficiency is not needed in the measurements reviewed in this work. However, for many configurations, such efficiency (η) can be characterized with high accuracy. Here, we take the TPET for elaboration. For an

electrically conductive sample of length L and diameter D, first, we can conduct the TET measurement to receive a steady-state resistance change of ΔR_1 under electrical heating of I_0^2R (I_0 is the current R is the resistance). Then, the TPET measurement is conducted for this sample under a laser intensity of I to receive a steady-state electrical resistance change of ΔR_2 . The final energy conversion efficiency can be readily calculated as $\eta = \Delta R_1 I_0^2 R/(\Delta R_2 LDI)$. Such a method provides a great way to characterize the optical energy absorption by micro/nanoscale materials and is a great feature of combined TET and TPET use.

B. Outlooks

In this paper, we reviewed various extensions of the photothermal idea for measuring thermophysical properties of materials, from macro- down to nanoscale size. The PA/PT techniques are capable of measuring coatings and suspended materials down to sub-µm thickness in the frequency domain. The phase shift method features high sensitivity than the amplitude method. In fact, the laser flash technique takes similar physics but probes the physics in the time domain. The TPET, PLTR, and PLTR2 techniques open a new way to measure micro/nanoscale materials with well-defined photon excitation and electrical thermal sensing. They provide great versatility in measuring 1D micro/nanoscale structures. The TDTR technique probes a material's thermal response by measuring its surface optical reflectance upon ultrafast pulsed heating. This technique is widely used for measuring coating-like materials but is unable to measure optically transparent materials (e.g., 2D materials) because it lacks the capability of materialspecific temperature sensing. The ET-Raman technique also is capable of ultrafast thermal probing but takes a strategy different from TDTR. Its great feature of material-specific thermal probing has found vast applications in measuring 2D materials.

These extended techniques based on the photothermal phenomenon always have their advantages and limitations. Their combination covers a very broad range of material measurements, from macro size down to atomic level. The PA/PT and TDTR techniques are quite mature, while great development rooms still exist for the ET-Raman, TPET, and PLTR2 techniques, especially for the ET-Raman technique. The main and urgent problem to be addressed is the thermal nonequilibrium between optical and acoustic phonons, which has been studied very little despite the pioneering work by Wang's group. Solving this problem will also help understand the energy coupling between phonon branches, which is critical to phonon engineering for various applications.

ACKNOWLEDGMENTS

Partial support for this work by the US National Science Foundation (Nos. CBET1930866 and CMMI2032464 for X.W.), National Natural Science Foundation of China (NSFC) (No. 52005367 for R.W. and No. 52106220 for S.X.), Guangdong Basic and Applied Basic Research Foundation (No. 2019A1515012183 for M.H. and No. 2020A1515110389 for J.L.), Natural Science Foundation of Top Talent of SZTU (No. 2019209 for J.L.) is gratefully acknowledged.

AUTHOR DECLARATIONS

Conflict of Interest

The authors have no conflicts to disclose.

Author Contributions

J.L., M.H., R.W., and S.X. contributed equally to this work.

DATA AVAILABILITY

The data that support the findings of this study are available from the corresponding author upon reasonable request and in the cited references.

REFERENCES

- ¹A. Rosencwaig and A. Gersho, J. Appl. Phys. 47, 64 (1976).
- ²S. D. Campbell, S. S. Yee, and M. A. Afromowitz, IEEE Trans. Biomed. Eng. 26, 220 (1979).
- ³C. A. Bennett and R. R. Patty, Appl. Opt. 21, 49 (1982).
- ⁴X. Wang, H. Hu, and X. Xu, J. Heat Trans. 123, 138 (2001).
- ⁵H. Hu, W. Zhang, J. Xu, and Y. Dong, Appl. Phys. Lett. **92**, 014103 (2008).
- ⁶H. Hu, X. Wang, and X. Xu, J. Appl. Phys. 86, 3953 (1999).
- ⁷Z. Xu, S. Xu, X. Tang, and X. Wang, AIP Adv. 4, 017131 (2014).
- ⁸S. Xu and X. Wang, AIP Adv. 4, 107122 (2014).
- ⁹X. Chen, Y. He, Y. Zhao, and X. Wang, Nanotechnology 21, 055707 (2010).
- 10X. Wang, Z. Zhong, and J. Xu, J. Appl. Phys. 97, 064302 (2005).
- ¹¹J. Guo, X. Wang, D. B. Geohegan, G. Eres, and C. Vincent, J. Appl. Phys. 103, 113505 (2008).
- 12 X. Feng, G. Liu, S. Xu, H. Lin, and X. Wang, Polymer 54, 1887 (2013).
- ¹³H. Lin, R. Wang, H. Zobeiri, T. Wang, S. Xu, and X. Wang, Nanoscale 13, 7723 (2021).
- ¹⁴R. Wang, H. Zobeiri, Y. Xie, X. Wang, X. Zhang, and Y. Yue, Adv. Sci. 7, 2000097 (2020).
- ¹⁵H. Zobeiri, R. Wang, T. Wang, H. Lin, C. Deng, and X. Wang, Int. J. Heat Mass Transfer 133, 1074 (2019).
- 16 J. Roegener, R. Brinkmann, and C. P. Lin, J. Biomed. Opt. 9, 367 (2004).
- ¹⁷J. Zhu, D. Tang, W. Wang, J. Liu, K. W. Holub, and R. Yang, J. Appl. Phys. 108, 094315 (2010).
- ¹⁸L. Li, H.-C. Hsu, V. V. Verkhusha, L. V. Wang, and D. M. Shcherbakova, Adv. Sci 8, 2102474 (2021).
- ¹⁹S. Quek, D. Almond, L. Nelson, and T. Barden, Meas. Sci. Technol. **16**, 1223 (2005).
- 20S. A. Telenkov, G. Vargas, J. S. Nelson, and T. E. Milner, Phys. Med. Biol. 47, 657 (2002).
- ²¹R. Mulaveesala and S. Tuli, Appl. Phys. Lett. **89**, 191913 (2006).
- ²²Y. Liu, W. Xiong, D. W. Li, Y. Lu, X. Huang, H. Liu, L. S. Fan, L. Jiang, J.-F. Silvain, and Y. F. Lu, Int. J. Extreme Manuf. 1, 025001 (2019).
- ²³M. Hasan, J. Zhao, and Z. Jiang, Int. J. Extreme Manuf. 1, 012004 (2019).
- ²⁴K. Krzempek, Appl. Sci. **9**, 2826 (2019).
- 25 P. Zhao, Y. Zhao, H. Bao, H. L. Ho, W. Jin, S. Fan, S. Gao, Y. Wang, and P. Wang, Nat. Commun. 11, 847 (2020).
- ²⁶D. G. Cahill, Rev. Sci. Instrum. **61**, 802 (1990).
- ²⁷D. G. Cahill and T. H. Allen, Appl. Phys. Lett. **65**, 309 (1994).
- ²⁸H. Hu, X. Wang, and X. Xu, J. Appl. Phys. **86**, 3953 (1999).
- ²⁹N. C. Fernelius, J. Appl. Phys. **51**, 650 (1980).
- **30**T. Fujii, K. Kumosaki, and M. Inoue, J. Appl. Phys. **52**, 2350 (1981).
- ³¹ J. Baumann and R. Tilgner, J. Appl. Phys. **58**, 1982 (1985).
- ³²T. Wang, X. Wang, Y. Zhang, L. Liu, L. Xu, Y. Liu, L. Zhang, Z. Luo, and K. Cen, J. Appl. Phys. **104**, 013528 (2008).
- ³³W. J. Parker, R. J. Jenkins, C. P. Butler, and G. L. Abbott, J. Appl. Phys. 32, 1679 (1961).

- ³⁴M. Sheindlin, D. Halton, M. Musella, and C. Ronchi, Rev. Sci. Instrum. 69, 1426 (1998).
- 35S.-K. Kim and Y.-J. Kim, Thermochim. Acta 468, 6 (2008).
- ³⁶H. Ohta, H. Shibata, A. Suzuki, and Y. Waseda, Rev. Sci. Instrum. **72**, 1899 (2001).
- 37 K. D. Cole and W. A. McGahan, J. Heat Transfer 115, 767 (1993).
- ³⁸H. Machlab, W. A. McGahan, J. A. Woollam, and K. Cole, Thin Solid Films 224, 22 (1993).
- ³⁹X. Wang, B. A. Cola, T. Bougher, S. L. Hodson, T. S. Fisher, and X. Xu, Annu. Rev. Heat Transfer 16, 135 (2013).
- ⁴⁰F. P. Incropera, D. P. DeWitt, and T. L. Bergman, Fundamentals of Heat and Mass Transfer (John Wiley, Hoboken, NJ, 2007).
- 41 T. Wang, X. Wang, J. Guo, Z. Luo, and K. Cen, Appl. Phys. A 87, 599 (2007).
- ⁴²H. Lin, S. Xu, X. Wang, and N. Mei, Small **9**, 2585 (2013).
- 43J. Liu, Z. Xu, Z. Cheng, S. Xu, and X. Wang, ACS Appl. Mater. Interfaces 7, 27279 (2015).
- 44Y, Xie, Z. Xu, S. Xu, Z. Cheng, N. Hashemi, C. Deng, and X. Wang, Nanoscale 7, 10101 (2015).
- 45 J. Q. Guo, X. W. Wang, and T. Wang, J. Appl. Phys. 101, 063537 (2007).
- 46Y. Xie, P. Yuan, T. Wang, N. Hashemi, and X. Wang, Nanoscale 8, 17581 (2016).
- ⁴⁷J. Q. Guo, X. W. Wang, D. B. Geohegan, and G. Eres, Funct. Mater. Lett. 1, 71 (2008).
- ⁴⁸M. Han, J. Liu, Y. Xie, and X. Wang, Carbon **126**, 532 (2018).
- ⁴⁹M. Han, Y. Xie, J. Liu, J. Zhang, and X. Wang, Nanotechnology 29, 265702 (2018).
- ⁵⁰D. G. Cahill, W. K. Ford, K. E. Goodson, G. D. Mahan, A. Majumdar, H. J. Maris, R. Merlin, and S. R. Phillpot, J. Appl. Phys. 93, 793 (2003).
- ⁵¹W. S. Capinski, H. J. Maris, T. Ruf, M. Cardona, K. Ploog, and D. S. Katzer, Phys. Rev. B **59**, 8105 (1999).
- ⁵²J. Zhu, D. W. Tang, W. Wang, J. Liu, K. W. Holub, and R. G. Yang, J. Appl. Phys. 108, 094315 (2010).
- ⁵³D. G. Cahill, Rev. Sci. Instrum. 75, 5119 (2004).
- 54 A. J. Schmidt, X. Y. Chen, and G. Chen, Rev. Sci. Instrum. 79, 114902 (2008).
 55 Y. Wang, J. V. Park, Y. K. Koh, and D. G. Cahill, J. Appl. Phys. 108, 04350
- 55Y. X. Wang, J. Y. Park, Y. K. Koh, and D. G. Cahill, J. Appl. Phys. 108, 043507 (2010).
- ⁵⁶D. L. Zhao, X. Qian, X. K. Gu, S. A. Jajja, and R. G. Yang, J. Electron. Packag. 138, 040802 (2016).
- $^{\bf 57}{\rm D.}$ G. Cahill, K. E. Goodson, and A. Majumdar, J. Heat Transfer 124, 223 (2002).
- ⁵⁸P. Q. Jiang, X. Qian, and R. Yang, Rev. Sci. Instrum. **88**, 074901 (2017).
- ⁵⁹D. G. Cahill, P. V. Braun, G. Chen, D. R. Clarke, S. H. Fan, K. E. Goodson, P. Keblinski, W. P. King, G. D. Mahan, A. Majumdar, H. J. Maris, S. R. Phillpot, E. Pop, and L. Shi, Appl. Phys. Rev. 1, 011305 (2014).

- ⁶⁰J. Y. Huang, J. Park, W. Wang, C. J. Murphy, and D. G. Cahill, ACS Nano 7, 3732 (2013).
- ⁶¹P. E. Hopkins, M. Baraket, E. V. Barnat, T. E. Beechem, S. P. Kearney, J. C. Duda, J. T. Robinson, and S. G. Walton, Nano Lett. 12, 590 (2012).
- 62 G. T. Hohensee, R. B. Wilson, and D. G. Cahill, Nat. Commun. 6, 6578 (2015).
- ⁶³J. Liu, S. H. Ju, N. Nishiyama, and S. Junichiro, Phys. Rev. B **100**, 064303 (2019).
- 64P. Jiang, X. Qian, X. Gu, and R. Yang, Adv. Mater. 29, 1701068 (2017).
- ⁶⁵H. J. Jang, J. D. Wood, C. R. Ryder, M. C. Hersam, and D. G. Cahill, Adv. Mater. 27, 8017 (2015).
- ⁶⁶Z. Luo, J. Maassen, Y. Deng, Y. Du, R. P. Garrelts, M. S. Lundstrom, P. D. Ye, and X. Xu, Nat. Commun. 6, 8572 (2015).
- and X. Xu, Nat. Commun. **6**, 8572 (2015).

 67X. Zhang, D. Sun, Y. Li, G. H. Lee, X. Cui, D. Chenet, Y. You, T. F. Heinz, and J. C. Hone, ACS Appl. Mater. Interfaces **7**, 25923 (2015).
- ⁶⁸X. F. Yue, Y. Y. Wang, Y. Zhao, J. Jiang, K. Yu, Y. Liang, B. Zhong, S. T. Ren, R. X. Gao, and M. Q. Zou, J. Appl. Phys. **127**, 104301 (2020).
- ⁶⁹M. Bergler, K. Cvecek, F. Werr, M. Brehl, D. De Ligny, and M. Schmidt, Int. J. Extreme Manuf. 2, 035001 (2020).
- 70 S. Xu, T. Wang, D. Hurley, Y. Yue, and X. Wang, Opt. Express 23, 10040 (2015).
- 71 C. Li, S. Xu, Y. Yue, B. Yang, and X. Wang, Carbon 103, 101 (2016).
- 72 T. Wang, S. Xu, D. H. Hurley, Y. Yue, and X. Wang, Opt. Lett. 41, 80 (2016).
- 73T. Wang, M. Han, R. Wang, P. Yuan, S. Xu, and X. Wang, J. Appl. Phys. 123, 145104 (2018).
- ⁷⁴R. Wang, H. Zobeiri, H. Lin, W. Qu, X. Bai, C. Deng, and X. Wang, Carbon 147, 58 (2019).
- ⁷⁵P. Yuan, R. Wang, T. Wang, X. Wang, and Y. Xie, Phys. Chem. Chem. Phys. 20, 25752 (2018).
- ⁷⁶H. Zobeiri, R. Wang, Q. Zhang, G. Zhu, and X. Wang, Acta Mater. 175, 222 (2019).
 ⁷⁷H. Zobeiri, N. Hunter, N. Van Velson, C. Deng, Q. Zhang, and X. Wang, Nano Energy 89, 106364 (2021).
- ⁷⁸H. Zobeiri, N. Hunter, R. Wang, T. Wang, and X. Wang, Adv. Sci. 8, 2004712 (2021).
- ⁷⁹N. Hunter, N. Azam, H. Zobeiri, R. Wang, M. Mahjouri-Samani, and X. Wang, ACS Appl. Mater. Interfaces 12, 51069 (2020).
- 80 S. Xu, A. Fan, H. Wang, X. Zhang, and X. Wang, Int. J. Heat Mass Transfer 154, 119751 (2020).
- 81 P. Yuan, J. Liu, R. Wang, and X. Wang, Nanoscale 9, 6808 (2017).
- 82P. Yuan, R. Wang, H. Tan, T. Wang, and X. Wang, ACS Photonics 4, 3115 (2017)
- ⁸³R. Wang, T. Wang, H. Zobeiri, P. Yuan, C. Deng, Y. Yue, S. Xu, and X. Wang, Nanoscale **10**, 23087 (2018).
- 84 P. Yuan, H. Tan, R. Wang, T. Wang, and X. Wang, RSC Adv. 8, 12767 (2018).
- 85 H. Zobeiri, S. Xu, Y. Yue, Q. Zhang, Y. Xie, and X. Wang, Nanoscale 12, 6064 (2020)